

Heavy-quark box-loop corrections to $q\bar{q} \rightarrow Z\gamma$ at two loops in QCD

Dario Kermanschah^{a,b,*} and Matilde Vicini^a

^a*Institute for Theoretical Physics, ETH Zurich, Wolfgang-Pauli-Strasse 27, 8093 Zürich, Switzerland*

^b*Rudolf Peierls Centre for Theoretical Physics, Oxford University, Clarendon Laboratory, Parks Road, Oxford OX1 3PU, UK*

E-mail: d.kermanschah@gmail.com, mvicini@phys.ethz.ch

We numerically compute the two-loop QCD corrections to $Z\gamma$ production at the LHC mediated by light- and heavy-quark box loops. The calculation employs the pipeline of refs. [1, 2], which performs Monte Carlo integration over spatial loop momenta after local subtraction of infrared, ultraviolet, and threshold singularities. We validate our results for partonic squared matrix elements with massless-quark loops against known benchmarks, extend them to include heavy-quark contributions, and compute the double-virtual corrections to $pp \rightarrow Z\gamma$ by performing the loop and phase space integrations simultaneously. This computation demonstrates the flexibility of the approach in handling both massless and massive final-state bosons, as well as additional mass scales in the loop.

17th International Symposium on Radiative Corrections: Applications of Quantum Field Theory to Phenomenology (RADCOR2025)

5-10 October 2025

Puri, India

*Speaker

1. Introduction

The computation of two-loop multi-leg scattering amplitudes with several external legs and multiple mass scales remains a major challenge in the field. In previous works [1, 2], we developed a numerical approach resilient to this level of complexity and demonstrated its feasibility by computing fermionic two-loop corrections to di- and triphoton production, involving up to eight independent kinematic and mass scales.

In these proceedings, we apply our techniques to the process $q\bar{q} \rightarrow Z\gamma$ mediated by light and heavy quark box loops. We exploit the fact that these contributions are kinematically equivalent to those where the Z boson is replaced by an off-shell photon. Therefore, the framework developed in ref. [2] applies directly to the production of a massless–massive boson pair. We recompute the two-loop squared matrix elements with massless quark loops and validate them against the analytic results of ref. [3]. In addition, we present new results for the contributions with heavy-quark box loops, for which no analytic benchmarks are currently available.

Our implementation can be directly used for cross section calculations of proton-proton scattering at the Large Hadron Collider (LHC) when combined with real-emission contributions. We illustrate this by computing the double-virtual corrections, convoluting the squared matrix element with parton distribution functions (PDFs), and performing the Monte Carlo integration over loop and phase space simultaneously.

In parallel work, we demonstrate that the same methods also apply to triangular fermion-loop corrections. These contributions vanish in massless quantum chromodynamics (QCD) but remain non-zero when heavy top and bottom quarks are present in the loop.

Our approach follows ref. [2] and constructs finite two-loop amplitudes in loop momentum space. It combines local infrared (IR) factorization at two loops [4–8] with local ultraviolet (UV) renormalization [9–11], before analytically integrating over the energy components of the loop momenta. This procedure leads to loop-tree duality representation [12–18], or equivalent but numerically more stable expressions arising from (partially) time-ordered perturbation theory [14, 15, 19–33]. The remaining threshold singularities are treated in accordance with the $i\epsilon$ causal prescription by subtracting them using the method of refs. [1, 2, 34, 35]. This approach improves control and numerical efficiency over contour deformation into the complex plane [30, 36–40]. The resulting expression is numerically integrated over spatial loop momenta, and if desired, over phase space, using a multi-channel Monte Carlo method with adaptive importance sampling based on the VEGAS algorithm [41–44].

2. Calculation

We consider the process

$$q(p_1) \bar{q}(p_2) \rightarrow \gamma(q_1) Z(q_2) \tag{1}$$

at two loops in QCD, focusing on the contribution mediated by box fermion loops in which a quark of flavor f with mass $m_f \geq 0$ circulates. The contributing Feynman diagrams with a single charge flow are shown in figure 1. The incoming quarks and outgoing photon are massless, $p_1^2 = p_2^2 = q_1^2 = 0$,

while the Z boson is massive, $q_2^2 > 0$. The coupling to quark vector and axial-vector currents is written as

$$ie\gamma^\mu(v_f^X - a_f^X\gamma^5), \quad X \in \{Z, \gamma\}, \quad (2)$$

where $e = \sqrt{4\pi\alpha}$ is the positron charge. For the Z boson, the couplings are expressed in terms of the weak mixing angle θ_W , the third component of weak isospin I_f^3 and the electric charge Q_f ,

$$v_f^Z = \frac{I_f^3 - 2s^2Q_f}{2sc}, \quad a_f^Z = \frac{I_f^3}{2sc}, \quad (3)$$

where $s = \sin\theta_W$ and $c = \cos\theta_W$. The photon couples only to the vector current,

$$v_f^\gamma = -Q_f, \quad a_f^\gamma = 0. \quad (4)$$

Charge conjugation invariance of the subprocess $gg \rightarrow Z\gamma$ implies that fermion loops with three vector and one axial coupling vanish. Hence, we can drop the axial coupling in the loop and compute the amplitude with vector couplings only, effectively replacing the Z boson with an off-shell photon γ^* up to the difference in their vector couplings. Therefore, the integrands constructed for ref. [2] for fermionic corrections to photon production can be reused here.

We denote the contribution to the two-loop scattering amplitude as

$$\left(\frac{\alpha_s}{4\pi}\right)^2 C_F T_F N_{Z\gamma} \delta_{ij} M^{(2, N_{Z\gamma})}, \quad (5)$$

where we factored out the strong coupling α_s , the color factors

$$C_F = \frac{N^2 - 1}{N}, \quad T_F = \frac{1}{2}, \quad (6)$$

with i and j the color indices of the incoming quark, and the quark vector couplings of the Z boson and photon summed over all equal-mass flavors:

$$N_{Z\gamma} = \sum_f e^2 v_f^Z v_f^\gamma. \quad (7)$$

The tree-level amplitude is

$$\delta_{ij} e^2 v_q^\gamma \left(v_q^Z M^{(0,V)} + a_q^Z M^{(0,A)} \right), \quad (8)$$

where we separated the vector and axial-vector contributions and factored out the corresponding couplings.

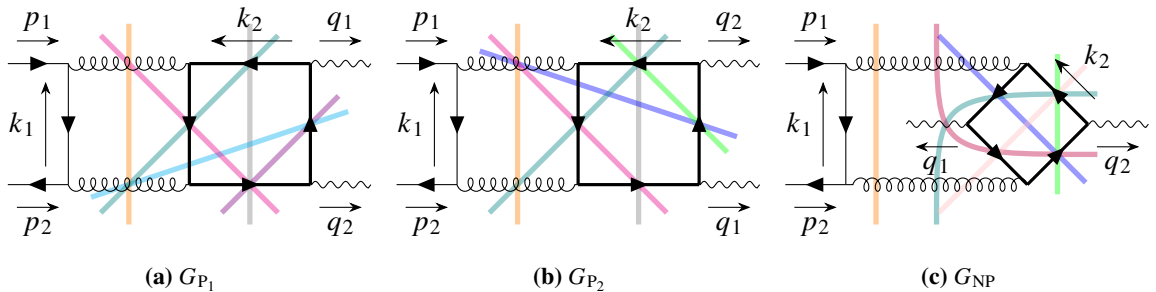


Figure 1: Planar and non-planar double box Feynman diagrams and their Cutkosky cuts identifying the threshold singularities. The diagrams with reversed charge flow are not shown.

2.1 IR and UV subtraction

The box-fermion loop corrections $M^{(2, N_{Z\gamma})}$ are finite in four spacetime dimensions, and neither require renormalization nor depend on the factorization scheme. However, the individual Feynman diagrams are IR and UV divergent. These divergences do not cancel locally in their sum but only globally after loop integration in dimensional regularization. To enable direct numerical integration in momentum space, we must first render the integrand power-counting finite by introducing local IR and UV counterterms.

We express each Feynman diagram in figure 1 as

$$G = \int \frac{d^d k_1}{\pi^{d/2}} \frac{d^d k_2}{\pi^{d/2}} \mathcal{G}, \quad (9)$$

and decompose the integrand in terms of its subgraphs,

$$\mathcal{G} = \mathcal{D}^{\alpha\beta} \mathcal{V}_{\alpha\beta}, \quad (10)$$

where the incoming quark line in Feynman gauge is

$$\mathcal{D}^{\alpha\beta} = i \frac{\bar{v}(p_2) \gamma^\beta (-\not{k}_1) \gamma^\alpha u(p_1)}{k_1^2 k_{g_1}^2 k_{g_2}^2}, \quad (11)$$

with gluon momenta k_{g_i} , and $\mathcal{V}_{\alpha\beta}$ denotes the fermion-loop subgraph. The $i\epsilon$ causal prescription in the Feynman propagators is left implicit.

The integral has divergences associated to longitudinal gluons collinear to the incoming massless quarks. Suitable IR counterterms were proposed in refs. [2, 4, 6]. Analogous to ref. [2], we subtract the two collinear limits $k \parallel p_i$ using the counterterms

$$\Delta_1 \mathcal{D}^{\alpha\beta} = -i \frac{\bar{v}(p_2) \gamma^\beta u(p_1)}{k_1^2 k_{g_1}^2} \frac{p_1 \cdot \zeta}{p_1 \cdot p_2} \frac{2k_{g_1}^\alpha}{(k_1 - \zeta)^2 - \zeta^2}, \quad (12)$$

$$\Delta_2 \mathcal{D}^{\alpha\beta} = -i \frac{\bar{v}(p_2) \gamma^\alpha u(p_1)}{k_1^2 k_{g_2}^2} \frac{p_2 \cdot \zeta}{p_1 \cdot p_2} \frac{-2k_{g_2}^\beta}{(k_1 - \zeta)^2 - \zeta^2}, \quad (13)$$

where ζ is an auxiliary vector satisfying $p_1 \cdot \zeta \neq 0$, $p_2 \cdot \zeta \neq 0$ and $\zeta^2 \neq 0$, which we choose as $\zeta = p_1 + p_2$.

UV divergences from the box-quark loops $\mathcal{V}_{\alpha\beta}$ are subtracted with UV counterterms constructed using the R -operation, which here corresponds to replacing the fermion propagator

$$\frac{i}{\not{k}_2 + \not{p} - m} \mapsto \frac{i \not{k}_2}{k_2^2 - M^2}, \quad (14)$$

where p is some momentum shift and M is a UV regulating mass. We note that the amplitude is independent of M as it is finite.

With these counterterms, each Feynman diagram becomes a finite integral in four dimensions:

$$\widehat{\mathcal{G}}^R = (1 - \Delta_1 - \Delta_2) \mathcal{D}^{\alpha\beta} (1 - R_{UV}) \mathcal{V}_{\alpha\beta}. \quad (15)$$

The Ward identity ensures that the sum of all IR counterterms integrates to zero [4, 6]. Moreover, the sum of UV counterterms reduces to the finite quantity after integrating over k_2 in dimensional regularization [4], leaving a finite one-loop integral over k_1 , which we also integrate numerically.

Finally, the amplitude can be expressed in terms of individually finite contributions:

$$M^{(2, N_{Z\gamma})} = 2 \left(\widehat{G}_{P_1}^R + \widehat{G}_{P_2}^R + \widehat{G}_{NP}^R \right) + R_{UV} M^{(2, N_{Z\gamma})}, \quad (16)$$

where the factor of two accounts for the diagrams with reversed charge flow, \widehat{G}_{P_i} and \widehat{G}_{NP} are the finite versions of the planar and non-planar diagrams in figure 1, and $R_{UV} M^{(2, N_{Z\gamma})}$ denotes the sum of UV counterterms.

2.2 Loop-energy integration and threshold subtraction

For each of the finite contributions above in eq. (16), we symbolically integrate over the energy components of the loop momenta using a FORM [45–47] script. The script first splits the propagators into linear denominators:

$$\frac{n(q^0)}{q^2 - m^2} = \frac{1}{2E} \left(\frac{n(E)}{q^0 - E} - \frac{n(-E)}{q^0 + E} \right) \quad (17)$$

where $n(q^0)$ is any linear numerator. It then applies partial fraction decomposition in the loop energies k_i^0 , such that only denominators with sums of on-shell energies are introduced, keeping only those terms in which a single simple pole in k_i^0 remains, which, if inside the chosen contour, integrates to its residue.

In general, this procedure can generate spurious singularities similar to those in time-ordered perturbation theory, involving sums of more than $n + 1$ on-shell energies for an n -loop integrand. Although spurious singularities of this type do not significantly affect numerical stability, we nonetheless checked that they did not arise in the contributions considered here. The resulting expressions are therefore equivalent to those obtained from partially time-ordered perturbation theory [23], the cross-free family [32], or causal loop-tree duality representations [26–29]. The practical advantage of our algorithm is that it operates entirely algebraically and does not require knowledge of an underlying graph structure.

The integrand after loop energy integration, which we denote by \mathcal{I} , still has threshold singularities, identified by the Cutkosky cuts illustrated in figure 1, e.g. the teal cut

$$t : \sqrt{(\vec{k}_1 - \vec{p}_2)^2} + \sqrt{(\vec{k}_1 + \vec{k}_2 + \vec{p}_1)^2 + m_f^2} + \sqrt{\vec{k}_2^2 + m_f^2} - p_1^0 - p_2^0 = 0. \quad (18)$$

If the quark mass m_f is sufficiently large, i.e. $q_2^2 < 4m_f^2$ or $s = (p_1 + p_2)^2 < 4m_f^2$ the final-state or s -channel cuts through the quark-loops do not admit solutions for real loop momenta. Each threshold singularity t is then subtracted using a counterterm:

$$C_t = \frac{\text{Res}[\mathcal{I}, r = r_t]}{r - r_t} \left(\frac{2r_t}{r + r_t} \right)^{6n-1}, \quad (19)$$

where r_t is the root of $t = 0$, and $r = |\mathbf{r}|$ is the magnitude of the n spatial loop momenta $\mathbf{r} = (\vec{k}_1, \dots, \vec{k}_n) + (\vec{s}_1, \dots, \vec{s}_n)$ with origin shifts \vec{s}_i .

Here, for the two-loop squared matrix elements, we take $\vec{s}_1 = \vec{p}_2$ in all cases, with $\vec{s}_2 = \vec{0}$ for planar and $\vec{s}_2 = \vec{q}_1/2$ for non-planar contributions. This choice is generally not suitable across the full phase space, so for the phase-space integrated virtual corrections we keep $\vec{s}_1 = \vec{p}_2$ and adjust \vec{s}_2 according to the region. If $q_2^2 > 4m_f^2$, we set $\vec{s}_2 = \vec{q}_1/2$ for both contributions. Otherwise, the planar case uses $\vec{s}_2 = \vec{0}$, while the non-planar employs two channels with sources $\vec{s}_2 = \vec{0}$ and $\vec{s}_2 = \vec{q}_1$, with singular surfaces separated as described in ref. [2]. All calculations are performed in the rest frame of $p_1 + p_2$.

The residue $\text{Res}[\mathcal{I}, r = r_t]$ corresponds to the product of the tree amplitudes separated by the cut. To avoid introducing a UV divergence, it is multiplied by a suppression function, constructed so that the Cauchy principal value integral vanishes. In eq. (19), this is ensured by antisymmetry under inversion, i.e.

$$f\left(\frac{r_t^2}{r^2}\mathbf{r}\right) = -\left(\frac{r_t^2}{r^2}\right)^{3n} f(\mathbf{r}), \quad (20)$$

although alternative UV suppression functions can be used (cf. [1, 34, 48]).

The dispersive part of the integral is obtained by integrating the subtracted integrand, $\mathcal{I} - \sum_t C_t$, over the spatial loop momenta, while the absorptive part comes from integrating the sum of residues over the $3n - 1$ dimensional space parameterized by $\hat{\mathbf{r}}$, where we can explicitly set the spacetime dimension to $d = 4$ and remove the $i\epsilon$ causal prescription.

For the process considered here, only the real part of the dispersive integral contributes to the squared matrix element. Therefore, in this case, though not in general, the imaginary part of the absorptive contribution can be neglected.

The integration over the energy components of the loop momenta, as well as the construction of the threshold counterterms is automated in our pipeline, previously used for the calculations in refs. [1, 2, 35]. We use SPENSO [49] and SYMBOLICA [50] to optimize the integrand expressions for fast evaluation.

3. Numerical results

We evaluate the helicity-summed squared matrix element

$$F^{(2, N_{Z\gamma})} = 2 \text{Re} \sum_h M_h^{(2, N_{Z\gamma})} \left(M_h^{(0, V)} \right)^*, \quad (21)$$

where the sum runs over the helicities h of the external particles. In our framework, it is obtained by multiplying the integrand of the dispersive part of our locally finite amplitude $M^{(2, \tilde{N}_f)}$ with the complex conjugate of the vector-contribution of tree amplitude $M_h^{(0, V)}$, summing over all helicities, and performing the numerical integration over the spatial loop momenta via Monte Carlo sampling.

We neglect the axial-vector coupling in the tree amplitude, as its contribution vanishes in the matrix element due to the absence of four linearly independent vectors to contract with the antisymmetric tensor $\epsilon^{\mu\nu\rho\sigma}$ generated by γ^5 . Exploiting parity invariance, we sum over only half the helicities and account for the other half with a factor of two.

We compute the squared matrix element for three randomly generated phase-space points, given in listing 1, at a center-of-mass energy $\sqrt{s} = 1000$ GeV, with $s = (p_1 + p_2)^2$ and using the

Process	PSP	Part	N_p [10^8]	Exp.	Reference	Result	Δ [σ]	Δ [%]
$q\bar{q} \rightarrow Z\gamma$ $m = 0$	1	$\widehat{F}_{P_1}^{(2,N_{Z\gamma}),R}$	5.2	10^{+2}		-3.2119 ± 0.0058		0.181
		$\widehat{F}_{P_2}^{(2,N_{Z\gamma}),R}$	5.2	10^{+2}		-3.5942 ± 0.0047		0.132
		$\widehat{F}_{NP}^{(2,N_{Z\gamma}),R}$	5.2	10^{+2}		4.2234 ± 0.0059		0.141
		$R_{UV}\widehat{F}^{(2,N_{Z\gamma})}$	5.2	10^{+1}		-6.4735 ± 0.0010		0.016
		$F^{(2,N_{Z\gamma})}$		10^{+2}	-5.8082	-5.8128 ± 0.0191	0.240	0.329
	2	$\widehat{F}_{P_1}^{(2,N_{Z\gamma}),R}$	5.2	10^{+2}		-3.5100 ± 0.0042		0.121
		$\widehat{F}_{P_2}^{(2,N_{Z\gamma}),R}$	5.2	10^{+2}		-3.2959 ± 0.0060		0.182
		$\widehat{F}_{NP}^{(2,N_{Z\gamma}),R}$	5.2	10^{+2}		4.3416 ± 0.0051		0.118
		$R_{UV}\widehat{F}^{(2,N_{Z\gamma})}$	5.2	10^{+1}		-6.4727 ± 0.0008		0.013
		$F^{(2,N_{Z\gamma})}$		10^{+2}	-5.5645	-5.5758 ± 0.0179	0.630	0.322
	3	$\widehat{F}_{P_1}^{(2,N_{Z\gamma}),R}$	8.2	10^{+2}		-2.6861 ± 0.0078		0.292
		$\widehat{F}_{P_2}^{(2,N_{Z\gamma}),R}$	5.2	10^{+2}		-3.8378 ± 0.0063		0.164
		$\widehat{F}_{NP}^{(2,N_{Z\gamma}),R}$	5.2	10^{+2}		3.7536 ± 0.0096		0.256
		$R_{UV}\widehat{F}^{(2,N_{Z\gamma})}$	5.2	10^{+1}		-6.4738 ± 0.0017		0.026
		$F^{(2,N_{Z\gamma})}$		10^{+2}	-6.2120	-6.1879 ± 0.0278	0.866	0.450

Table 1: Helicity-summed squared matrix element (in bold), defined in eq. (21), together with the planar, non-planar, and UV counterterm contributions introduced in eq. (16), evaluated at the three phase-space points given in listing 1, for the two-loop corrections involving massless-quark box loops. The reference results were obtained from the analytic amplitudes computed in ref. [3].

physical Z boson mass $m_Z = 91.1876$ GeV, such that $q_2^2 = m_Z^2$. We set the UV mass parameter to $M = \sqrt{s}$. Table 1 shows the contribution from massless quark-loops, which we verified against the analytic computation of ref. [3]. Table 2 displays the contributions from bottom- and top-quark loops, using $m_b = 4.18$ GeV and $m_t = 172$ GeV.

In the table headers, N_p denotes the number of Monte Carlo samples, Δ [%] the relative error in percent and Δ [σ] the deviation from the reference value (where available) expressed in units of the Monte Carlo error. To our knowledge, no benchmark results for these massive contributions are available in the literature. State-of-the-art analytic results for two-loop (massless) diphoton amplitudes with heavy-quark loops, involving one fewer mass scale than our process, were presented in refs. [51, 52] and used as a benchmark in our earlier work [2].

Alongside the squared matrix element, the table reports the planar, non-planar, and UV counterterm contributions defined in eq. (16). These components were summed and their Monte Carlo errors combined in quadrature, to obtain the squared matrix element. Since the UV counterterms do not depend on the mass of the quark in the loop, their values are identical in all cases and are shown for completeness.

Process	PSP	Part	N_p [10^8]	Exp.	Result	Δ [%]
$q\bar{q} \rightarrow Z\gamma$ $m = m_b$	1	$\widehat{F}_{P_1}^{(2,N_{Z\gamma}),R}$	5.2	10^{+2}	-3.2121 ± 0.0055	0.171
		$\widehat{F}_{P_2}^{(2,N_{Z\gamma}),R}$	5.2	10^{+2}	-3.5921 ± 0.0037	0.104
		$\widehat{F}_{NP}^{(2,N_{Z\gamma}),R}$	5.2	10^{+2}	4.1129 ± 0.0043	0.104
		$R_{UV}\widehat{F}^{(2,N_{Z\gamma})}$	5.2	10^{+1}	-6.4735 ± 0.0010	0.016
		$F^{(2,N_{Z\gamma})}$		10^{+2}	-6.0300 ± 0.0158	0.262
	2	$\widehat{F}_{P_1}^{(2,N_{Z\gamma}),R}$	5.2	10^{+2}	-3.5063 ± 0.0037	0.105
		$\widehat{F}_{P_2}^{(2,N_{Z\gamma}),R}$	5.2	10^{+2}	-3.3003 ± 0.0047	0.142
		$\widehat{F}_{NP}^{(2,N_{Z\gamma}),R}$	5.2	10^{+2}	4.2485 ± 0.0039	0.092
		$R_{UV}\widehat{F}^{(2,N_{Z\gamma})}$	5.2	10^{+1}	-6.4727 ± 0.0008	0.013
		$F^{(2,N_{Z\gamma})}$		10^{+2}	-5.7634 ± 0.0142	0.247
	3	$\widehat{F}_{P_1}^{(2,N_{Z\gamma}),R}$	5.8	10^{+2}	-2.7072 ± 0.0081	0.299
		$\widehat{F}_{P_2}^{(2,N_{Z\gamma}),R}$	5.2	10^{+2}	-3.8490 ± 0.0047	0.123
		$\widehat{F}_{NP}^{(2,N_{Z\gamma}),R}$	5.2	10^{+2}	3.5838 ± 0.0059	0.166
		$R_{UV}\widehat{F}^{(2,N_{Z\gamma})}$	5.2	10^{+1}	-6.4738 ± 0.0017	0.026
		$F^{(2,N_{Z\gamma})}$		10^{+2}	-6.5922 ± 0.0222	0.337
$q\bar{q} \rightarrow Z\gamma$ $m = m_t$	1	$\widehat{F}_{P_1}^{(2,N_{Z\gamma}),R}$	5.2	10^{+2}	-5.3468 ± 0.0022	0.042
		$\widehat{F}_{P_2}^{(2,N_{Z\gamma}),R}$	5.2	10^{+2}	-4.5173 ± 0.0016	0.035
		$\widehat{F}_{NP}^{(2,N_{Z\gamma}),R}$	5.2	10^{+2}	9.3880 ± 0.0018	0.019
		$R_{UV}\widehat{F}^{(2,N_{Z\gamma})}$	5.2	10^{+1}	-6.4735 ± 0.0010	0.016
		$F^{(2,N_{Z\gamma})}$		10^{+2}	-1.5996 ± 0.0065	0.407
	2	$\widehat{F}_{P_1}^{(2,N_{Z\gamma}),R}$	5.2	10^{+2}	-4.4679 ± 0.0016	0.035
		$\widehat{F}_{P_2}^{(2,N_{Z\gamma}),R}$	5.2	10^{+2}	-4.9993 ± 0.0021	0.042
		$\widehat{F}_{NP}^{(2,N_{Z\gamma}),R}$	5.2	10^{+2}	9.0230 ± 0.0016	0.017
		$R_{UV}\widehat{F}^{(2,N_{Z\gamma})}$	5.2	10^{+1}	-6.4727 ± 0.0008	0.013
		$F^{(2,N_{Z\gamma})}$		10^{+2}	-1.5356 ± 0.0061	0.399
	3	$\widehat{F}_{P_1}^{(2,N_{Z\gamma}),R}$	5.2	10^{+2}	-6.4309 ± 0.0031	0.049
		$\widehat{F}_{P_2}^{(2,N_{Z\gamma}),R}$	5.2	10^{+2}	-4.8192 ± 0.0018	0.037
		$\widehat{F}_{NP}^{(2,N_{Z\gamma}),R}$	5.2	10^{+3}	1.0681 ± 0.0003	0.024
		$R_{UV}\widehat{F}^{(2,N_{Z\gamma})}$	5.2	10^{+1}	-6.4738 ± 0.0017	0.026
		$F^{(2,N_{Z\gamma})}$		10^{+2}	-1.7862 ± 0.0089	0.497

Table 2: Helicity-summed squared matrix element (in bold), defined in eq. (21), together with the planar, non-planar, and UV counterterm contributions introduced in eq. (16), evaluated at the three phase-space points given in listing 1, for the two-loop corrections with top- and bottom-quark box loops.

Process	Part	N_p [10^8]	Exp.	Result	Δ [%]
$pp \rightarrow Z\gamma$ $m = 0$	$\widehat{\sigma}_P^{(2,N_{Z\gamma}),R}$	262.9	10^{-5}	8.0566 ± 0.0028	0.035
	$\widehat{\sigma}_{NP}^{(2,N_{Z\gamma}),R}$	108.3	10^{-4}	-1.6398 ± 0.0006	0.035
	$R_{UV}\widehat{\sigma}^{(2,N_{Z\gamma})}$	5.2	10^{-5}	2.2703 ± 0.0006	0.027
	$\sigma^{(2,N_{Z\gamma})}$		10^{-5}	1.7005 ± 0.0161	0.945
$pp \rightarrow Z\gamma$ $m = m_b$	$\widehat{\sigma}_P^{(2,N_{Z\gamma}),R}$	37.0	10^{-5}	8.1366 ± 0.0071	0.087
	$\widehat{\sigma}_{NP}^{(2,N_{Z\gamma}),R}$	17.9	10^{-4}	-1.5434 ± 0.0009	0.058
	$R_{UV}\widehat{\sigma}^{(2,N_{Z\gamma})}$	5.2	10^{-5}	2.2703 ± 0.0006	0.027
	$\sigma^{(2,N_{Z\gamma})}$		10^{-5}	3.9486 ± 0.0334	0.846
$pp \rightarrow Z\gamma$ $m = m_t$	$\widehat{\sigma}_P^{(2,N_{Z\gamma}),R}$	33.6	10^{-5}	3.5718 ± 0.0012	0.035
	$\widehat{\sigma}_{NP}^{(2,N_{Z\gamma}),R}$	10.4	10^{-5}	-7.8350 ± 0.0027	0.034
	$R_{UV}\widehat{\sigma}^{(2,N_{Z\gamma})}$	5.2	10^{-5}	2.2703 ± 0.0006	0.027
	$\sigma^{(2,N_{Z\gamma})}$		10^{-6}	8.8753 ± 0.0735	0.828

Table 3: Double-virtual corrections as defined in eq. (22) mediated by light- and heavy-quark loops, including the planar, non-planar and UV counterterms contributions defined through eq. (16). Collision energy, transverse momentum cuts, and PDF specifications are given in the text.

Because the bottom-quark mass is small, its contribution is numerically close to the massless result, particularly for the planar box diagrams. Differences are more visible in the non-planar contributions, leading to percent-level effects in the squared matrix element. In contrast, the large top-quark mass significantly modifies both the analytic structure and the numerical result: only s -channel threshold singularities remain as the final-state thresholds are absent.

We also evaluate the double-virtual corrections that enter the $pp \rightarrow Z\gamma$ cross section, by convoluting the squared matrix element with the PDFs and integrating over the phase space:

$$\sigma^{(2,N_{Z\gamma})} = \sum_q \int dx_1 dx_2 f_q(x_1, \mu_F) f_{\bar{q}}(x_2, \mu_F) v_q^Z v_q^\gamma \frac{F^{(2,N_{Z\gamma})}(x_1 x_2 s)}{2x_1 x_2 s} \mathcal{O}, \quad (22)$$

where $f_{q,\bar{q}}(x_{1,2}, \mu_F)$ are the PDFs of the incoming (anti-)quarks at factorization scale μ_F and momentum fractions $x_{1,2}$, respectively. By $d\Pi_2$ we denote the 2-body phase space measure and \mathcal{O} is an observable function. We perform the Monte Carlo integration simultaneously over spatial loop momentum, phase space and momentum fractions. Here, except for $v_q^Z v_q^\gamma$, all other couplings and color factors (as in eqs. (5) and (8)) are excluded from $\sigma^{(2,N_{Z\gamma})}$, which is also not averaged over spin helicities.

The presence of heavy-quark thresholds depends on the center-of-mass energy, and, when integrating over the Bjorken variables, the overlap structure of the threshold surfaces changes. Compared to ref. [2], this required minor structural modifications to our pipeline, enabling the

# PSP1				
0.5000000000000000E+03	0.0000000000000000E+00	0.0000000000000000E+00	0.5000000000000000E+03	
0.5000000000000000E+03	0.0000000000000000E+00	0.0000000000000000E+00	-0.5000000000000000E+03	
0.4958424108776996E+03	0.1100019292470276E+03	0.4411319421848414E+03	-0.1978936117492713E+03	
0.5041575891223005E+03	-0.1100019292470276E+03	-0.4411319421848414E+03	0.1978936117492712E+03	
# PSP2				
0.5000000000000000E+03	0.0000000000000000E+00	0.0000000000000000E+00	0.5000000000000000E+03	
0.5000000000000000E+03	0.0000000000000000E+00	0.0000000000000000E+00	-0.5000000000000000E+03	
0.4958424108776997E+03	-0.2795713281286689E+03	-0.3875414700574890E+03	0.1323298072962480E+03	
0.5041575891223005E+03	0.2795713281286690E+03	0.3875414700574891E+03	-0.1323298072962480E+03	
# PSP3				
0.5000000000000000E+03	0.0000000000000000E+00	0.0000000000000000E+00	0.5000000000000000E+03	
0.5000000000000000E+03	0.0000000000000000E+00	0.0000000000000000E+00	-0.5000000000000000E+03	
0.4958424108776987E+03	-0.2386202223474536E+03	0.2781398312686913E+03	-0.3340034732958395E+03	
0.5041575891223014E+03	0.2386202223474535E+03	-0.2781398312686913E+03	0.3340034732958395E+03	

Listing 1: Three phase-space points for $q(p_1)\bar{q}(p_2) \rightarrow \gamma(q_1)Z(q_2)$ with $m_Z = 91.1876$ GeV at a center-of-mass energy of $\sqrt{s} = 1000$ GeV.

dynamic activation of the relevant threshold counterterms and a more flexible choice of their parameterization, so that the double-virtual corrections with heavy-quark loops can be integrated numerically over the full phase space.

In table 3, we show the phase-space integrated double-virtual corrections defined in eq. (22) along with the planar, non-planar and UV counterterm contributions defined according to eq. (16). Due to symmetry, the phase-space integrated contributions from the two planar double box integrals are identical, which we denote by $\widehat{\sigma}_{\text{P}}^{(2,N_{Z\gamma}),R} = \widehat{\sigma}_{\text{P}_1}^{(2,N_{Z\gamma}),R} = \widehat{\sigma}_{\text{P}_2}^{(2,N_{Z\gamma}),R}$ in the table. We aimed for below 1% precision on the double-virtual corrections, but significantly higher accuracy was needed for the planar and non-planar contributions due to cancellations¹. We also point out the significantly larger number of samples required for the massless quark-loop contributions compared to the massive ones.

We set the center-of-mass energy to $\sqrt{s} = 13$ TeV and the factorization scale and UV mass to $\mu_F = M = m_Z = 91.1876$ GeV. The observable \mathcal{O} imposes a phase-space cut requiring minimal transverse momenta of $p_T^{\text{min}} = 50$ GeV for the photon and 25 GeV for the Z boson. We use the CT10 NLO PDF set [53] from LHAPDF [54] with five light flavors (u, d, c, s, b) and convolute it with the squared matrix elements, including massless-quark loops and heavy bottom- and top-quark box loops with $m_b = 4.18$ GeV and $m_t = 172$ GeV.

¹It would be beneficial to realize these cancellations locally before loop integration, although this has not been investigated further.

Process	$\widehat{F}_{\text{P}_1}^{(2,N_{Z\gamma}),R}$	$\widehat{F}_{\text{P}_2}^{(2,N_{Z\gamma}),R}$	$\widehat{F}_{\text{NP}}^{(2,N_{Z\gamma}),R}$	$R_{\text{UV}}\widehat{F}^{(2,N_{Z\gamma})}$
$q\bar{q} \rightarrow Z\gamma, m = 0$	0.646	0.627	0.674	0.022
$q\bar{q} \rightarrow Z\gamma, m = m_b$	1.807	1.423	1.917	0.022
$q\bar{q} \rightarrow Z\gamma, m = m_t$	1.632	1.293	1.394	0.022

Table 4: Single-core integrand evaluation times in milliseconds using double-precision arithmetic averaged over 10^4 samples. In contrast to ref. [2], expression optimization was performed only at the level of individual diagrams rather than for their combined expression, leading to slightly longer evaluation times.

The numerical integration is carried out using a multi-channel Monte Carlo method with the parameterizations described in ref. [2]. To ensure numerical stability, each phase-space sample is reevaluated using an equivalent rotated momentum configuration in double precision. If fewer than seven digits agree, the point is recomputed in double-double precision [55, 56]. All Monte Carlo integrations were performed on the Euler computing cluster at ETH Zurich. Average evaluation times per sample, benchmarked on a single core of an AMD EPYC 7763 processor, are shown in table 4.

4. Conclusion

In this work, we applied the numerical techniques and implementation of ref. [2] to compute the two-loop QCD corrections with light- and heavy-quark box loops to $q\bar{q} \rightarrow Z\gamma$. We validated the massless QCD result by comparing it with the analytic calculation of ref. [3] and provided new results available for the heavy-quark contributions.

We further performed the convolution with PDFs and integrated over the phase space, obtaining the corresponding double-virtual corrections to $Z\gamma$ production in proton–proton collisions at the LHC.

These results highlight the flexibility of our numerical approach, which can accommodate contributions to different processes and treat multiple mass scales within a unified computational framework. Moreover, the method is capable of providing phase-space integrated corrections with sufficient precision to enable phenomenological studies when combined with real-emission contributions, as available in ref. [57–60].

We are currently extending this framework to compute the remaining two-loop contributions.

Acknowledgments

We thank the organizers of RADCOR 2025 for the opportunity to present our work and for their hospitality. We acknowledge the use of the Euler cluster at ETH Zurich for the numerical computations. This work was supported by the Swiss National Science Foundation through its Postdoc.Mobility funding scheme (grant number 230593) and project funding scheme (grant number 10001706).

References

- [1] D. Kermanschah and M. Vicini, N_f -contribution to the virtual correction for electroweak vector boson production at NNLO, *JHEP* **09** (2025) 213 [2407.18051].
- [2] D. Kermanschah and M. Vicini, Two-loop QCD corrections for real and off-shell diphoton and triphoton production via quark loops, 2510.18801.
- [3] T. Gehrmann and L. Tancredi, Two-loop QCD helicity amplitudes for $q\bar{q} \rightarrow W^\pm\gamma$ and $q\bar{q} \rightarrow Z^0\gamma$, *JHEP* **02** (2012) 004 [1112.1531].
- [4] C. Anastasiou, R. Haindl, G. Sterman, Z. Yang and M. Zeng, Locally finite two-loop amplitudes for off-shell multi-photon production in electron-positron annihilation, *JHEP* **04** (2021) 222 [2008.12293].
- [5] C. Anastasiou and G. Sterman, Locally finite two-loop QCD amplitudes from IR universality for electroweak production, *JHEP* **05** (2023) 242 [2212.12162].
- [6] C. Anastasiou, J. Karlen, G. Sterman and A. Venkata, Locally finite two-loop amplitudes for electroweak production through gluon fusion, *JHEP* **11** (2024) 043 [2403.13712].
- [7] C. Anastasiou, J. Karlen, R. Sahoo, G. Sterman and M. Vicini, General finite two-loop amplitude integrand for photoproduction in quark annihilation, 2509.07805.
- [8] C. Anastasiou, J. Karlen, Y. Ma and G. Sterman, Local finiteness for real-virtual corrections to electroweak production in partonic collisions, 2601.22936.
- [9] N.N. Bogoliubov and O.S. Parasiuk, On the Multiplication of the causal function in the quantum theory of fields, *Acta Math.* **97** (1957) 227.
- [10] K. Hepp, Proof of the Bogolyubov-Parasiuk theorem on renormalization, *Commun. Math. Phys.* **2** (1966) 301.
- [11] W. Zimmermann, Convergence of Bogolyubov's method of renormalization in momentum space, *Commun. Math. Phys.* **15** (1969) 208.
- [12] S. Catani, T. Gleisberg, F. Krauss, G. Rodrigo and J.-C. Winter, From loops to trees by-passing Feynman's theorem, *JHEP* **09** (2008) 065 [0804.3170].
- [13] J.J. Aguilera-Verdugo, F. Driencourt-Mangin, J. Plenter, S. Ramírez-Uribe, G. Rodrigo, G.F.R. Sborlini et al., Causality, unitarity thresholds, anomalous thresholds and infrared singularities from the loop-tree duality at higher orders, *JHEP* **12** (2019) 163 [1904.08389].
- [14] J.J. Aguilera-Verdugo, F. Driencourt-Mangin, R.J. Hernández-Pinto, J. Plenter, S. Ramirez-Uribe, A.E. Renteria Olivo et al., Open Loop Amplitudes and Causality to All Orders and Powers from the Loop-Tree Duality, *Phys. Rev. Lett.* **124** (2020) 211602 [2001.03564].

- [15] J. Jesús Aguilera-Verdugo, R.J. Hernández-Pinto, G. Rodrigo, G.F.R. Sborlini and W.J. Torres Bobadilla, *Mathematical properties of nested residues and their application to multi-loop scattering amplitudes*, *JHEP* **02** (2021) 112 [2010.12971].
- [16] S. Ramírez-Uribe, R.J. Hernández-Pinto, G. Rodrigo and G.F.R. Sborlini, *From Five-Loop Scattering Amplitudes to Open Trees with the Loop-Tree Duality*, *Symmetry* **14** (2022) 2571 [2211.03163].
- [17] R. Runkel, Z. Szőr, J.P. Vesga and S. Weinzierl, *Causality and loop-tree duality at higher loops*, *Phys. Rev. Lett.* **122** (2019) 111603 [1902.02135].
- [18] Z. Capatti, V. Hirschi, D. Kermanschah and B. Ruijl, *Loop-Tree Duality for Multiloop Numerical Integration*, *Phys. Rev. Lett.* **123** (2019) 151602 [1906.06138].
- [19] G.T. Bodwin, *Factorization of the Drell-Yan Cross-Section in Perturbation Theory*, *Phys. Rev. D* **31** (1985) 2616.
- [20] J.C. Collins, D.E. Soper and G.F. Sterman, *Factorization for Short Distance Hadron - Hadron Scattering*, *Nucl. Phys. B* **261** (1985) 104.
- [21] G.F. Sterman, *An Introduction to quantum field theory*, Cambridge University Press (8, 1993).
- [22] G.F. Sterman, *Partons, factorization and resummation, TASI 95*, in *Theoretical Advanced Study Institute in Elementary Particle Physics (TASI 95): QCD and Beyond*, pp. 327–408, 6, 1995 [hep-ph/9606312].
- [23] G. Sterman and A. Venkata, *Local infrared safety in time-ordered perturbation theory*, *JHEP* **02** (2024) 101 [2309.13023].
- [24] J.J. Aguilera-Verdugo, R.J. Hernandez-Pinto, G. Rodrigo, G.F.R. Sborlini and W.J. Torres Bobadilla, *Causal representation of multi-loop Feynman integrands within the loop-tree duality*, *JHEP* **01** (2021) 069 [2006.11217].
- [25] S. Ramírez-Uribe, R.J. Hernández-Pinto, G. Rodrigo, G.F.R. Sborlini and W.J. Torres Bobadilla, *Universal opening of four-loop scattering amplitudes to trees*, *JHEP* **04** (2021) 129 [2006.13818].
- [26] G.F.R. Sborlini, *Geometrical approach to causality in multiloop amplitudes*, *Phys. Rev. D* **104** (2021) 036014 [2102.05062].
- [27] W.J. Torres Bobadilla, *Loop-tree duality from vertices and edges*, *JHEP* **04** (2021) 183 [2102.05048].
- [28] W.J.T. Bobadilla, *Lotty – The loop-tree duality automation*, *Eur. Phys. J. C* **81** (2021) 514 [2103.09237].
- [29] P. Benincasa and W.J.T. Bobadilla, *Physical representations for scattering amplitudes and the wavefunction of the universe*, *SciPost Phys.* **12** (2022) 192 [2112.09028].

- [30] S. Kromin, N. Schwanemann and S. Weinzierl, *Amplitudes within causal loop-tree duality*, *Phys. Rev. D* **106** (2022) 076006 [2208.01060].
- [31] Z. Capatti, V. Hirschi, D. Kermanschah, A. Pelloni and B. Ruijl, *Manifestly Causal Loop-Tree Duality*, 2009.05509.
- [32] Z. Capatti, *Exposing the threshold structure of loop integrals*, *Phys. Rev. D* **107** (2023) L051902 [2211.09653].
- [33] Z. Capatti, *Derivation of the Cross-Free Family representation for the box diagram*, *PoS RADCOR2023* (2024) 027 [2311.14374].
- [34] D. Kermanschah, *Numerical integration of loop integrals through local cancellation of threshold singularities*, *JHEP* **01** (2022) 151 [2110.06869].
- [35] M. Vicini and D. Kermanschah, *Numerical integration of the double- and triple-box integrals using threshold subtraction*, *PoS LL2024* (2024) 078 [2407.21511].
- [36] D.E. Soper, *Techniques for QCD calculations by numerical integration*, *Phys. Rev. D* **62** (2000) 014009 [hep-ph/9910292].
- [37] S. Becker, D. Goetz, C. Reuschle, C. Schwan and S. Weinzierl, *NLO results for five, six and seven jets in electron-positron annihilation*, *Phys. Rev. Lett.* **108** (2012) 032005 [1111.1733].
- [38] S. Becker, C. Reuschle and S. Weinzierl, *Efficiency Improvements for the Numerical Computation of NLO Corrections*, *JHEP* **07** (2012) 090 [1205.2096].
- [39] S. Buchta, G. Chachamis, P. Draggiotis and G. Rodrigo, *Numerical implementation of the loop-tree duality method*, *Eur. Phys. J. C* **77** (2017) 274 [1510.00187].
- [40] Z. Capatti, V. Hirschi, D. Kermanschah, A. Pelloni and B. Ruijl, *Numerical Loop-Tree Duality: contour deformation and subtraction*, *JHEP* **04** (2020) 096 [1912.09291].
- [41] G.P. Lepage, *Adaptive multidimensional integration: VEGAS enhanced*, *J. Comput. Phys.* **439** (2021) 110386 [2009.05112].
- [42] G.P. Lepage, *A New Algorithm for Adaptive Multidimensional Integration*, *J. Comput. Phys.* **27** (1978) 192.
- [43] T. Hahn, *CUBA: A Library for multidimensional numerical integration*, *Comput. Phys. Commun.* **168** (2005) 78 [hep-ph/0404043].
- [44] B. Ruijl, “havana: A rust monte carlo integrator that supports discrete and continuous dimensions and nested grids.” <https://github.com/benruijl/havana>, 2025.
- [45] J. Kuipers, T. Ueda and J.A.M. Vermaseren, *Code Optimization in FORM*, *Comput. Phys. Commun.* **189** (2015) 1 [1310.7007].

- [46] B. Ruijl, J. Vermaseren, A. Plaats and J.v.d. Herik, *Combining Simulated Annealing and Monte Carlo Tree Search for Expression Simplification*, [1312.0841](#).
- [47] J. Davies, T. Kaneko, C. Marinissen, T. Ueda and J.A.M. Vermaseren, *FORM Version 5.0*, [2601.19982](#).
- [48] W. Kilian and T. Kleinschmidt, *Numerical Evaluation of Feynman Loop Integrals by Reduction to Tree Graphs*, [0912.3495](#).
- [49] M. Fraaije, V. Hirschi, L. Huber and B. Ruijl, “Spenso.”
<https://github.com/alpha100p/spenso/releases/tag/spynso3-v0.1.0>, 2024.
- [50] B. Ruijl, *Symbolica*, Sept., 2025. [10.5281/zenodo.17054381](#).
- [51] M. Becchetti, F. Coro, C. Nega, L. Tancredi and F.J. Wagner, *Analytic two-loop amplitudes for $q\bar{q} \rightarrow \gamma\gamma$ and $gg \rightarrow \gamma\gamma$ mediated by a heavy-quark loop*, *JHEP* **06** (2025) 033 [[2502.00118](#)].
- [52] T. Ahmed, A. Chakraborty, E. Chaubey and M. Kaur, *Two-loop helicity amplitudes for diphoton production with massive quark loop*, *JHEP* **12** (2025) 106 [[2502.03282](#)].
- [53] H.-L. Lai, M. Guzzi, J. Huston, Z. Li, P.M. Nadolsky, J. Pumplin et al., *New parton distributions for collider physics*, *Phys. Rev. D* **82** (2010) 074024 [[1007.2241](#)].
- [54] A. Buckley, J. Ferrando, S. Lloyd, K. Nordström, B. Page, M. Rüfenacht et al., *LHAPDF6: parton density access in the LHC precision era*, *Eur. Phys. J. C* **75** (2015) 132 [[1412.7420](#)].
- [55] M. Joldes, J.-M. Muller and V. Popescu, *Tight and rigorous error bounds for basic building blocks of double-word arithmetic*, *ACM Trans. Math. Softw.* **44** (2017) .
- [56] A. Tribick, J.L. Cruz and A. Pelloni, “twofloat.”
<https://github.com/apelloni/twofloat/tree/dev>, 2026.
- [57] M. Grazzini, S. Kallweit and M. Wiesemann, *Fully differential NNLO computations with MATRIX*, *Eur. Phys. J. C* **78** (2018) 537 [[1711.06631](#)].
- [58] M. Grazzini, S. Kallweit, D. Rathlev and A. Torre, *$Z\gamma$ production at hadron colliders in NNLO QCD*, *Phys. Lett. B* **731** (2014) 204 [[1309.7000](#)].
- [59] M. Grazzini, S. Kallweit and D. Rathlev, *$W\gamma$ and $Z\gamma$ production at the LHC in NNLO QCD*, *JHEP* **07** (2015) 085 [[1504.01330](#)].
- [60] J.M. Campbell, T. Neumann and C. Williams, *$Z\gamma$ Production at NNLO Including Anomalous Couplings*, *JHEP* **11** (2017) 150 [[1708.02925](#)].